

Microscopic model for FitzHugh-Nagumo dynamics

Anatoly Malevanets and Raymond Kapral

Chemical Physics Theory Group, Department of Chemistry, University of Toronto, Toronto, Ontario, Canada M5S 3H6

(Received 13 September 1996)

A microscopic reaction model with a FitzHugh-Nagumo mass action law is introduced. A Markov chain that uses a birth-death description of the reaction mechanism and a random walk model for diffusion is constructed and implemented as a lattice-gas automaton. It is shown that the local particle density probability distribution is binomial in the high diffusion limit and the average particle density is governed by the FitzHugh-Nagumo reaction-diffusion equation. The lattice-gas simulations are able to reproduce phenomena such as labyrinthine patterns and Bloch fronts predicted to exist on the basis of the reaction-diffusion equation. The effects of fluctuations on these chemical patterns, the breakdown of the mass-action and reaction-diffusion descriptions, and the existence of phase transitions in the strong reaction limit are discussed. [S1063-651X(97)13703-5]

PACS number(s): 82.20.Wt, 05.40.+j, 05.60.+w, 51.10.+y

I. INTRODUCTION

The FitzHugh-Nagumo equation [1]

$$\begin{aligned} u_\tau &= -u^3 + u - v, \\ v_\tau &= \epsilon(u - \alpha v - \beta), \end{aligned} \quad (1)$$

was originally constructed as a simple model for the excitable behavior of nerve tissue. It mimics the behavior of the more realistic Hodgkin-Huxley equations, and while the u and v variables may be roughly associated with the membrane voltage and ion currents, respectively, their connection with these physiological variables is not direct. Although the antecedents of this model lie in physiology, it has seen widespread use as a generic model that exhibits many phenomena seen in bistable, excitable, or oscillatory chemical media. The existence of S-shaped and linear nullclines are features common to many systems and allow for the possibility of a variety of dynamical states. In its spatially distributed form as a reaction-diffusion equation,

$$\begin{aligned} u_\tau &= -u^3 + u - v + D_u \nabla^2 u, \\ v_\tau &= \epsilon(u - \alpha v - \beta) + D_v \nabla^2 v, \end{aligned} \quad (2)$$

it has been used to study spiral wave dynamics in excitable media [2] as well as the varied front bifurcation phenomena [3–5] seen in recent chemical experiments on the iodide-ferrocyanide-sulfite system [6]. In this latter case the ratio of the two diffusion coefficients plays an important role as a bifurcation parameter.

Given this rich phenomenology, it is of interest to construct a microscopic dynamics whose mean-field limit is the FitzHugh-Nagumo equation (1). From a knowledge of such microscopic dynamics a statistical mechanics that underlies the pattern formation processes seen in this system may be constructed and the effects of correlations and fluctuations on the dynamics may be studied.

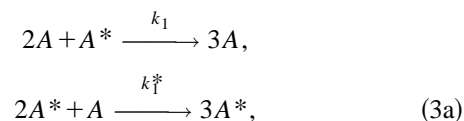
We depart from the standard interpretation of the FitzHugh-Nagumo (FHN) model in terms of nerve impulse physiology and devise a chemical scheme whose mass-action law is the FHN equation (1). The reaction mechanism and reduction to FHN kinetics are discussed in Sec. II. We con-

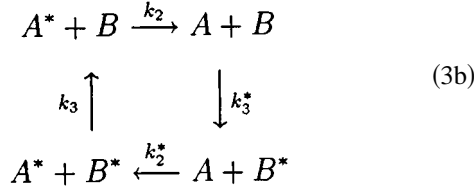
struct a microscopic collision dynamics corresponding to the mechanism and implement it in the context of a lattice-gas automaton [7]. The automaton construction is described in Sec. III. A formulation of the stochastic Markov chain dynamics underlying the model is given in Sec. IV. In this section we also discuss the conditions under which the microscopic dynamics reduces to the reaction-diffusion equation. In Sec. V we demonstrate that the microscopic dynamics can reproduce the known front bifurcation phenomena seen in the reaction-diffusion equation. In Sec. VI we consider the effects of small fluctuations on the pattern formation processes, as well as the breakdown of the reaction-diffusion equation when reaction is sufficiently fast that a local equilibrium description of the dynamics is no longer applicable. Noise-induced phase transitions are examined in some detail. The conclusions of this study are given in Sec. VII.

II. FITZHUGH-NAGUMO REACTION KINETICS

A particular chemical mechanism is not usually associated with FHN kinetics; in fact, the linear inhibition of u by the v variable poses problems for normal kinetic schemes. However, it is possible to devise such a mechanism and an essential feature is its cooperative nature: the reaction steps not only depend on the local numbers of particles of the species but also on the numbers of vacancies or ‘holes’ corresponding to the species.

We consider a two-variable, site-specific, reaction scheme where active sites can accommodate a maximum of N molecules of species A and B . The vacancies corresponding to these species will be denoted by A^* and B^* , respectively. The mechanism comprises two processes: a relaxation of the system toward either one of the pure A states where sites are either completely filled with A or completely empty of A , and a cyclic mechanism involving coupling of the A and B species. The mechanism reads





The cooperative kinetics arising from the dependence on the number of vacancies as well as the number of actual molecules present at a site has some features in common with biochemical reactions involving the cooperative binding of substrate molecules to an enzyme in a complex of allosteric enzymes [8] or to reactions on surfaces which depend on the existence of vacancies [9]. This reaction scheme is to be interpreted in the usual sense of mechanisms for systems constrained to lie far from equilibrium, namely, feed species whose values are fixed by flows of reagents into and out of the system are not explicitly indicated and their constant concentrations are incorporated in the values of the rate constants. Consequently, the model does not satisfy detailed balance and this is responsible for its rich mean-field phenomenology.

Examining the mechanism, one can see that if the density of A particles exceeds that of the vacancies creation of A particles prevails over creation of vacancies. The first step in Eq. (3a) supports the formation of pure phase A with sites completely filled and the second step favors a situation where sites are completely empty. In contrast to the effect of Eq. (3a), the cyclic series of steps in Eq. (3b) accounts for the interaction between the A and B species and favors the formation of site states composed of both particles and vacancies. This leads to competition between the pure bistable states and gives rise to phenomena which are more complex than simple bistability.

The mass-action rate law that follows from Eq. (3) is

$$\begin{aligned}
 a_t &= \{k_1 a - k_1^*(1-a)\}a(1-a) + k_2(1-a)b - k_2^*a(1-b) \\
 &\equiv R_A(a,b), \\
 b_t &= k_3(1-a)(1-b) - k_3^*ab \equiv R_B(a,b), \quad (4)
 \end{aligned}$$

where a and b are the average concentrations per site of species A and B , respectively. If the rate constants satisfy $k_2 = k_2^*$ and $k_3 = k_3^*$ and one makes use of the change of variables $a = c_a u + a_0$ and $b = c_b v + b_0$ where

$$\begin{aligned}
 c_a^2 &= \frac{1}{3} \left(\frac{k_1 + 2k_1^*}{k_1 + k_1^*} \right)^2 - \frac{k_2 + k_1^*}{k_1 + k_1^*}, \quad a_0 = \frac{1}{3} \frac{k_1 + 2k_1^*}{k_1 + k_1^*}, \\
 c_b &= \frac{k_1 + k_1^*}{k_2} c_a^2, \quad b_0 = a_0 c_b \left\{ 1 - \left(\frac{a_0}{c_a} \right)^2 \right\}, \quad (5)
 \end{aligned}$$

and the scaled time variable $\tau = t/\tau_s$, with $\tau_s^{-1} = (k_1 + k_1^*)c_a^2$, one recovers the FHN rate law (1). The parameters in (1) are related to the rate constants by

$$\alpha = \frac{c_b}{c_a}, \quad \beta = \frac{b_0 - a_0}{c_a}, \quad \epsilon = \frac{k_3}{k_2} \frac{c_a}{c_b}. \quad (6)$$

Using these results, the rate constants in the mechanism can be tuned to yield desired values of the FHN parameters.

III. LATTICE-GAS MODEL

Once a chemical mechanism is known it is possible to devise a microscopic reactive collision dynamics that accounts for the steps in the mechanism. We consider the implementation of the mechanism as a reactive lattice-gas automaton and give descriptions in terms of a Markov chain model in Sec. IV. Reactive lattice-gas models provide a Markov chain description of the dynamics. They utilize a birth-death description of local reactive events at the lattice nodes, while particle diffusion arises from the random walks the particles execute on the lattice [10].

We begin by introducing the notation used in the construction of the model. The coordinate space for the lattice-gas model is a regular Bravais lattice \mathcal{L} of elementary sites ℓ . Each site is occupied by some number of particles. The occupation numbers of the different species are independent of each other so that the space of all possible site configurations \mathcal{B} is a direct product of particle states $\mathcal{B} = \otimes_{\kappa} Z_{s_{\kappa}}$, where s_{κ} is the maximum number of states for species “ κ ” and $Z_s = \{n \in \mathbb{Z} | 0 \leq n < s\}$. The maximum number of molecules of species κ is N_{κ} and, henceforth, we assume that $N_{\kappa} = N$ for all κ . A lattice state is a distribution of particles on the lattice and is given by a mapping $\mathbb{L}: \mathcal{L} \rightarrow \mathcal{B}$. The space of all possible lattice states is denoted by $\Omega = \mathcal{B}^{\mathcal{L}}$. The distribution of particles of only one species will be termed a lattice substate and we designate lattice states and substates with blackboard bold letters (e.g., for species A the lattice substate is \mathbb{A}). The lattice state \mathbb{L} is the collection of lattice substates for all species A, B, \dots , $\mathbb{L} = (\mathbb{A}, \mathbb{B}, \dots)$ and each site ℓ is defined by a set of site occupation numbers $\ell = (n, m, \dots)$, where we use n for the particle number of species A , m for species B , etc. The value of a state or substate S at a lattice point \mathbf{r} is designated by $S(\mathbf{r})$.

The evolution of a lattice state is governed by operators acting on Ω . We restrict ourselves to operators defined as a composition of collision and translation operators. The collision operators naturally arise from the representation of a lattice state as a mapping onto \mathcal{B} . For any site operator $\sigma: \mathcal{B} \rightarrow \mathcal{B}'$ there corresponds a lattice operator $C_{\sigma} = \sigma \circ \mathcal{L}: \mathcal{L} \rightarrow \mathcal{B}'$. These operators act on each site independently. Interactions between sites are accomplished by translation operators which act on the lattice substates by translating the particles in a chosen direction. Translation of a lattice substate S in a direction \mathbf{v} is given by

$$S(\mathbf{r} + \mathbf{v}) = T_{\mathbf{v}} S(\mathbf{r}). \quad (7)$$

Its action yields a change of the coordinate origin of the lattice substate.

A. Brownian motion

We describe Brownian motion by the collective movement in a random direction of an ensemble of randomly chosen particles. In some implementations of diffusion rules in lattice-gas models particles are assigned velocities and propagate in directions determined by these velocities to neighboring lattice nodes where the velocities are random-

ized [10]. An exact solution for the linear Markov process for this scheme shows that these random walkers are effectively noninteracting and are binomially distributed. The model used here is different and makes use of an auxiliary “excited” particle lattice substate \mathbb{E} and simulates diffusion by a three-step algorithm: (a) transfer of at most one particle per site to the excited state with a probability depending on the site occupation number; (b) translation of the excited particles in a random direction chosen from a set $V = \{\mathbf{v}_1, \dots, \mathbf{v}_k\}$; (c) accommodation of the excited particles at new positions. The fact that only a maximum of N particles of each species may reside at a node (exclusion principle) requires a vacancy to exist at a site in order to be able to accommodate a particle from the excited sublattice; in addition, we cannot create an excited particle from the vacuum, so that we have two restrictions on the excitation probability: $p(N)=1$ and $p(0)=0$. We shall show in the Sec. IV that the choice of a linear dependence of the excitation probability on the site occupation number leads to a concentration independent diffusion coefficient.

Consider the Brownian motion of particles of species A . The lattice state comprises substates of species A , \mathbb{A} , and the auxiliary “excited” state species E , \mathbb{E} . Formally, if the maximum occupation number is N , the above algorithm may be expressed as the composition of three operators

$$D = C_\alpha \circ T_v \circ C_\tau \quad (8)$$

where T_v is a translation of the lattice substate \mathbb{E} in a randomly chosen direction \mathbf{v} , while C_τ and C_α are lattice operators corresponding to the following site operators:

$$\tau(n, e) = (n - \theta(n - N\xi), \theta(n - N\xi)), \quad \alpha(n, e) = (n + e, 0), \quad (9)$$

where $\theta(x)$ is the Heaviside function, n is the number of molecules of species A at a site, and ξ is a continuous, uniformly distributed, random variable on $(0,1)$. The operator τ in Eq. (9) corresponds to step (a) and transfers a particle to the excited state while the operator α places an excited particle in a new position determined by the action of the translation operator. The algorithm is well defined since at each step the occupation number of each species is no greater than N and is nonnegative; $\mathbb{E} \leq \mathbb{A}$ on the first step and $\mathbb{E} \leq 1 \wedge \mathbb{A} < N$ on the last.

In the Sec. IV we shall show that when correlations between sites are neglected the above scheme leads to an isotropic diffusion equation. The isotropy does not arise from the symmetry of the underlying lattice but is a property of the Laplacian operator in the diffusion equation. Due to this feature it suffices to consider a random walk on a square lattice for two dimensions and on a cubic lattice for three dimensions. However, in the presence of correlations this isotropy can be broken and to regain it one should utilize lattices with symmetry groups larger than those of cubic lattices; e.g., the triangular lattice for two-dimensional systems and the projection of the four-dimensional fcc lattice for three-dimensional problems [11]. In simulations reported in this paper we used a cubic lattice and a set of directions from a four-dimensional fcc lattice for the three-dimensional computations and a nine-direction scheme, obtained by projecting the fcc velocity directions on a plane, for two-

dimensional simulations. We note that the discrete diffusion operator Δ has nonsymmetric terms of second order in the lattice spacing.

B. Reactive dynamics

We now construct a two-species microscopic collision model which will be shown in Sec. IV to lead to the FitzHugh-Nagumo equations in the Boltzmann approximation. As earlier, we label species sublattices by \mathbb{A} and \mathbb{B} so that the lattice state is given by $\mathbb{L} = (\mathbb{A}, \mathbb{B})$ (apart from excited sublattice states used in the diffusion rule). Each site is defined by the set of occupation variables $\mathcal{L} = (n, m)$ where n and m are the numbers of molecules of species A and B at a site. The reaction rule is carried out by randomly choosing one of the $r=6$ channels in the mechanism (3) where each channel is assigned an equal weight. A reactive event requires a pair of random numbers (ξ, ν) , where ξ is a continuous, uniformly distributed, random number on $(0,1)$ and ν is a discrete, uniformly distributed, random number on $\{1, \dots, r\}$.

The local reactive dynamics at a node occurs by birth-death processes arising from the $r=6$ steps in the reaction mechanism. The reaction probabilities p_j corresponding to each of these six steps are

$$\begin{aligned} p_1(n, m) &= \gamma \bar{k}_1 n(n-1)(N-n), \\ p_2(n, m) &= \gamma \bar{k}_1^* n(N-n)(N-1-n), \\ p_3(n, m) &= \gamma \bar{k}_2(N-n)m, \quad p_4(n, m) = \gamma \bar{k}_2^* n(N-m), \\ p_5(n, m) &= \gamma \bar{k}_3^* (N-n)(N-m), \quad p_6(n, m) = \gamma \bar{k}_3 nm, \end{aligned} \quad (10)$$

where γ is a scale factor that controls the overall time scale of the reaction process and $\bar{k}_1 = k_1 / [(N-1)(N-2)]$, $\bar{k}_1^* = k_1^* / [(N-1)(N-2)]$ and $\bar{k}_i = k_i / N$ and $\bar{k}_i^* = k_i^* / N$ for $i=2,3$ where k_i and k_i^* are the reaction rate coefficients defined earlier. In writing this set of probabilities we have labeled the steps $j=[1,6]$ in the reaction mechanism characterized by k_i and k_i^* as follows: $j=2i-1$ for reactions labeled by k_i and $j=2i$ for reactions labeled by k_i^* . Site operators corresponding to the different channels are easily written in terms of these reaction probabilities and are given below

$$\begin{aligned} \sigma_1(n, m) &= (n + \theta(p_1 - \xi), m) , \\ \sigma_2(n, m) &= (n - \theta(p_2 - \xi), m) , \\ \sigma_3(n, m) &= (n + \theta(p_3 - \xi), m) , \\ \sigma_4(n, m) &= (n - \theta(p_4 - \xi), m) , \\ \sigma_5(n, m) &= (n, m + \theta(p_5 - \xi)) , \\ \sigma_6(n, m) &= (n, m - \theta(p_6 - \xi)) . \end{aligned}$$

We note that all of the operations are legitimate in the following sense: if the reaction rule creates a particle, a vacancy

exists; if a particle was destroyed, it existed prior to destruction. The local reaction rule has the following site operator expression:

$$\rho(n,m) = \sum_{j=1}^6 \delta_{vj} \sigma_j(n,m) , \quad (11)$$

and C_ρ is the corresponding lattice operator on $L=(A,B)$. An important feature of the above scheme is that the reactive transitions among molecules and vacancies are such that the exclusion principle is satisfied automatically.

IV. SITE MARKOV CHAIN DESCRIPTION

The lattice-gas rules constitute a Markov chain description of the dynamics on the finite lattice. In order to analyze the model in some detail we make the approximation that the full probability distribution is the product of single site probability distributions. For reaction, no approximation is involved since reactions occur independently on each lattice node. Correlations arising from exclusion are neglected in the diffusion rule, but we shall demonstrate that these are numerically small by comparison with simulation results.

A. Diffusion Markov chain

We now show that the evolution of the average particle density defined by the Brownian motion algorithm is approximated by a diffusion equation. In the analysis we assume that there is no correlation between lattice sites; hence, the probability distribution function is equal to a product of reduced site probability distributions. This assumption will be verified below by comparison with simulations. Let $P_n(\mathbf{r},t)$ be the probability of finding n molecules of species A at the site \mathbf{r} at time t . The evolution of the reduced probability density is described by the following Markov chain

$$P_n(\mathbf{r},t+1) - P_n(\mathbf{r},t) = \sum_{n'} W_{nn'}^D(\mathbf{r}) P_{n'}(\mathbf{r},t) , \quad (12)$$

where, using the random walk rule outlined in Sec. III A, $W_{nn'}^D(\mathbf{r})$ is given by

$$\begin{aligned} W_{nn'}^D = & \bar{a} \left(1 - \frac{n'}{N} \right) \delta_{n',n-1} + (1-\bar{a}) \frac{n'}{N} \delta_{n',n+1} \\ & - \left[\bar{a} \left(1 - \frac{n'}{N} \right) + (1-\bar{a}) \frac{n'}{N} \right] \delta_{n',n} , \end{aligned} \quad (13)$$

which depends on the average density in the neighborhood of the point \mathbf{r} ,

$$\bar{n}(\mathbf{r},t) = \frac{1}{2d} \sum_{\mathbf{r}' \in \mathcal{N}(\mathbf{r})} \sum_n n P_n(\mathbf{r}',t) = \frac{1}{2d} \sum_{\mathbf{r}' \in \mathcal{N}(\mathbf{r})} \langle n \rangle(\mathbf{r}',t) , \quad (14)$$

(d is the dimensionality) with $\bar{a}(\mathbf{r},t) = \bar{n}(\mathbf{r},t)/N$. [We have dropped the arguments of $\bar{a}(\mathbf{r},t)$ for notational simplicity.] Multiplying Eq. (12) by n and summing on n we obtain an equation for the evolution of the expectation value of the particle number

$$\begin{aligned} \langle n \rangle(\mathbf{r},t+1) - \langle n \rangle(\mathbf{r},t) &= \frac{1}{2dN} \sum_{\mathbf{r}' \in \mathcal{N}(\mathbf{r})} [\langle n \rangle(\mathbf{r}',t) - \langle n \rangle(\mathbf{r},t)] \\ &= \frac{1}{2dN} \Delta \langle n \rangle(\mathbf{r},t) , \end{aligned} \quad (15)$$

where Δ is a discrete Laplacian operator. This is just a discrete version of the diffusion equation with diffusion coefficient $D=1/2dN$.

The stationary probability distribution of Eq. (12) is binomial. To show this it is convenient to consider the generating function [12] of the distribution

$$F(x,\mathbf{r},t) = \sum_{n=0}^N P_n(\mathbf{r},t) x^n . \quad (16)$$

Using this definition and Eq. (12) we find

$$\begin{aligned} F(x,\mathbf{r},t+1) - F(x,\mathbf{r},t) &= \left\{ -\bar{a}(1-x) + \frac{(1-x)}{N} [1-\bar{a}(1-x)] \frac{\partial}{\partial x} \right\} F(x,\mathbf{r},t) . \end{aligned} \quad (17)$$

The stationary, spatially homogeneous, generating function $F(x)$ is given by the solution of

$$\left\{ -a(1-x) + \frac{(1-x)}{N} [1-a(1-x)] \frac{\partial}{\partial x} \right\} F(x) = 0 , \quad (18)$$

which is $F(x) = [1-a(1-x)]^N$, with $a = \langle n \rangle / N$. This is the generating function for a binomial distribution $p_n^B = \binom{N}{n} a^n (1-a)^{N-n}$.

The above analysis hinges on the approximation that the distribution function for the lattice is the product distribution over lattice sites. Consequently, it is of interest to compare the site distribution function obtained by direct simulation of the diffusion rule, which makes no assumption about independence or correlations, with that predicted from the Markov chain (12). The results of numerical simulations show that correlations among sites are negligible over the entire range of average particle densities and that the stationary distribution is well described by a binomial distribution. By analogy with the expression for the factorial cumulants of a discrete random variable n one may construct an expression for the generating function that gives only one nonvanishing cumulant for a binomial distribution. For the function

$$\sqrt[N]{\langle (1+x)^n \rangle} - 1 = \sum_{j=1}^{\infty} \langle \langle n \rangle \rangle_j \frac{x^j}{j!} \quad (19)$$

the first factorial cumulant is equal to the average density and for a binomial distribution the other cumulants are zero. In the limit $N \rightarrow \infty$ the above expression is proportional to the standard expression for the factorial cumulants [12]. Computations yield the following values for the cumulants: $\langle \langle n \rangle \rangle_1 = 0.35$, $\langle \langle n \rangle \rangle_2 = 8.5 \times 10^{-5}$, and $\langle \langle n \rangle \rangle_3 = 2.2 \times 10^{-4}$ confirming that correlations are indeed small. In Fig. 1 cumulants computed over a range of average densities are com-

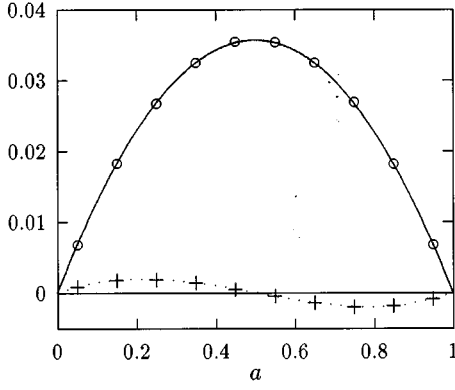


FIG. 1. Second (○) and third (+) cumulants compared with their theoretical values $a(1-a)/N$ (solid line) and $a(2a-1)(a-1)/N^2$ (dotted line).

pared with cumulants of a binomial distribution. The values coincide for all average particle densities.

It is important to determine how quickly a binomial distribution is established at a node and to do this one needs an estimate of the relaxation eigenvalues of the transition matrix of the Markov chain. We suppose that the average density of the neighboring sites is fixed at the value a and study the evolution of the site probability density to a binomial distribution with density a . Using the continuous-time version of Eq. (17) with $\bar{a}(\mathbf{r}, t) = a$ and making the change of variable $z = 1 - x$ and $F(x, t) = f(z, t)$ we have

$$\frac{\partial f(z, t)}{\partial t} = - \left\{ az + (1 - az) \frac{z}{N} \frac{\partial}{\partial z} \right\} f(z, t) . \quad (20)$$

Equation (20) is equivalent to the following system of ordinary differential equations:

$$t_{\mu} = 1 , \quad z_{\mu} = \frac{(1 - az)z}{N} , \quad f_{\mu} = -azf , \quad (21)$$

with initial conditions at $\mu = 0$ constrained by a curve parameterized by variable ζ

$$t = 0 , \quad z = \zeta , \quad f = \omega(\zeta)(1 - a\zeta)^N . \quad (22)$$

Solution of the system of equations (21) passing through the surface (22) is

$$t = \mu , \quad \ln \left(\frac{az}{1 - az} \right) = \frac{\mu}{N} + \ln \left(\frac{a\zeta}{1 - a\zeta} \right) ,$$

$$\ln(f) = N \ln(1 - az) + \omega(\zeta) . \quad (23)$$

Elimination of the variables μ and ζ from the above system gives the following solution of Eq. (20):

$$f(z, t) = (1 - az)^N \omega \left(\frac{z}{\exp(t/N)(1 - az) + az} \right) . \quad (24)$$

From this equation we may read off the second largest eigenvalue $\lambda_1^D = -(1/N)$. The average particle number relaxes to a stationary value as

$$\langle n \rangle(t) = - \left. \frac{\partial f}{\partial z} \right|_{z=0} = Na - e^{-t/N} \left. \frac{\partial \omega(x)}{\partial x} \right|_{x=0} , \quad (25)$$

where we used condition $f|_{z=0} = 1$, which must always be imposed on a generating function of a probability distribution.

The characteristic diffusion length L_{λ} associated with the relaxation time $1/|\lambda_1^D| = N$ is $L_{\lambda} = \sqrt{DN}$ or, noting that $D = 1/2dN$, $L_{\lambda} = 1/\sqrt{2d}$ which is of the order of a lattice spacing. Consequently, the system will quickly relax to a local binomial distribution and one will be able to resolve phenomena on the spatial scale of the lattice maintaining this local binomial distribution. This result will be used in the subsequent analysis.

B. Reaction Markov chain

The microscopic, single-site, reaction dynamics can be written as a Markov chain. Let $P_{nm}(t)$ be the probability of finding n molecules of species A and m molecules of species B at a site. In view of the birth-death description of the reaction process at a site this probability satisfies the evolution equation,

$$P_{nm}(t+1) - P_{nm}(t) = \sum_{n', m'} W_{nm, n'm'}^R P_{n'm'}(t) , \quad (26)$$

where

$$W_{nm, n'm'}^R = (p_1(n', m') + p_3(n', m')) \delta_{n, n'+1} \delta_{m', m}$$

$$+ (p_2(n', m') + p_4(n', m')) \delta_{n, n'-1} \delta_{m', m}$$

$$+ p_5(n', m') \delta_{n', n} \delta_{m, m'+1}$$

$$+ p_6(n', m') \delta_{n', n} \delta_{m, m'-1}$$

$$- \left(\sum_{i=1}^r p_i(n', m') \right) \delta_{n', n} \delta_{m', m} . \quad (27)$$

To obtain the generating function for the reaction we use the procedure described earlier for the diffusion model. There are two major differences: first, the distribution function for reaction cannot be factored into a product of distribution functions for the A and B species and second, due to absence of site interactions, the equation for the stationary distribution function is linear. The generating function for the probability distribution function is

$$F(x, y, t) = \sum_{0 \leq n, m \leq N} P_{nm}(t) x^n y^m . \quad (28)$$

Each reaction channel provides a contribution to the evolution equation for the generating function and using Eqs. (26) and (28) we find

$$F(x, y, t+1) - F(x, y, t) = \sum_{j=1}^6 C^{(j)}(x, y, t) \equiv C(x, y, t) , \quad (29)$$

where $C^{(j)}(x, y, t)$ is the contribution from channel j . Computing these reactive terms explicitly we find

$$\begin{aligned}
C(x,y) = & \bar{k}_1(1-x)x^{N+1} \left[\frac{F_{xx}}{x^{N-2}} \right]_x + \bar{k}_1^*(1-x)x^N \left[\frac{F_x}{x^{N-2}} \right]_{xx} \\
& + \bar{k}_2(1-x)x^{N+1}y \left[\frac{F}{x^N} \right]_{xy} - \bar{k}_2^*(1-x)y^{N+1} \left[\frac{F}{y^N} \right]_{xy} \\
& + \bar{k}_3(1-y)x F_{xy} - \bar{k}_3^*(1-y)(xy)^{N+1} \left[\frac{F}{(yx)^N} \right]_{xy} .
\end{aligned} \tag{30}$$

The rates of change of the average particle densities are given by $a(t+1) - a(t) = C_x(1,1,t)/N$ and $b(t+1) - b(t) = C_y(1,1,t)/N$. The condition for the probability distribution function to be a stationary distribution function is tantamount to the condition that the sum of all reaction terms vanish. Equation (30) is quite difficult to solve analytically and it is more rewarding to solve the underlying linear system for P_{nm} . We shall return to this expression in Sec. IV C as well as in Sec. VI where the breakdown of the mean-field and reaction-diffusion results are considered.

If one assumes diffusive mixing is strong, so that the system is spatially homogeneous and the distribution is a product of binomial distributions for the A and B species, Eq. (30) is easily evaluated. Using the generating function for a binomial distribution function we have

$$F(x,y) = (1+a(x-1))^N (1+b(y-1))^N . \tag{31}$$

Substituting this expression into Eq. (30) and evaluating the derivatives, we find $C_x(1,1,t)/N = R_A(a,b)$ and $C_y(1,1,t)/N = R_B(a,b)$, where $R_A(a,b)$ and $R_B(a,b)$ are the mass-action rates given in Eq. (4). Thus, we verify that the mass-action rate law is found in this strong diffusion limit when reactive correlations at a node are neglected.

We may confirm that the microscopic model yields results in agreement with the mass-action rate law in the strong diffusion limit. In Fig. 2 we compare the stationary average densities obtained from simulations of the lattice-gas model with those obtained from the mean-field equations. The mean-field steady states are given by stationary solutions of Eq. (4). The reaction rate difference expressed as a function of average density may be written as follows:

$$k_1 - k_1^* = (2a - 1) \left[k_1 + k_1^* - \frac{2k_2}{a(1-a)} \right] . \tag{32}$$

This equation yields a van der Waals loop. As the relative stability of the stable states (defined by the difference in rate coefficients $k_1 - k_1^*$) changes, the system undergoes a first order phase transition. The position of the transition is defined by the analog of a Maxwell rule and in this case corresponds to equal rate coefficients. The simulation results were obtained by varying $k_1 - k_1^*$ from negative to positive values while keeping $k_1 + k_1^*$ constant. We observed hysteresis when varying $k_1 - k_1^*$ from positive to negative values. The average steady state densities are in good agreement with the mass-action law results.

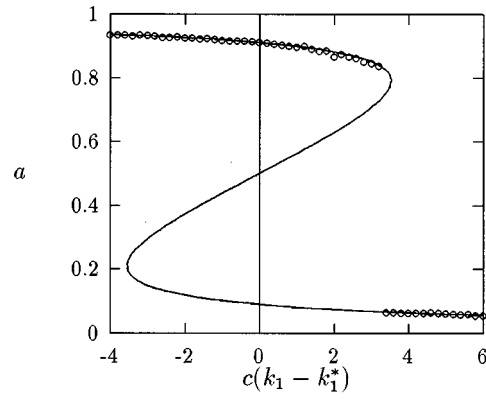


FIG. 2. Steady state densities in the bistable regime as a function of the rate coefficient difference $k_1 - k_1^*$. The line represents the FHN mass-action model and the points correspond to the ‘‘A’’-particle densities from simulations. Parameter values of Eq. (4) corresponding to $k_1 = k_1^*$ are $\epsilon = 0.127$, $\alpha = 5.12$, and $\beta = 0.0$. The simulation results were obtained by varying $k_1 - k_1^*$ from negative to positive values. The simulations were carried out on a $23 \times 23 \times 23$ lattice. The scaling constant c for the abscissa is $c = 8.167$.

C. Reaction-diffusion equation

In the independent-site approximation, the Markov chain describing both reaction and diffusion is obtained by combining the reaction and diffusion steps described individually above. The Markov chain may be written in matrix form as

$$\mathbf{P}(\mathbf{r}, t+1) = (\mathbf{W}^D + \mathbf{1})(\gamma \mathbf{W}^R + \mathbf{1})\mathbf{P}(\mathbf{r}, t) , \tag{33}$$

where the parameter γ can be used to gauge the relative magnitudes of the reaction and diffusion time scales. If both diffusion and reaction probabilities are small, we may expand the matrix product to linear order to obtain,

$$\mathbf{P}(\mathbf{r}, t+1) - \mathbf{P}(\mathbf{r}, t) = (\mathbf{W}^D + \gamma \mathbf{W}^R)\mathbf{P}(\mathbf{r}, t) \equiv \mathbf{W}\mathbf{P}(\mathbf{r}, t) , \tag{34}$$

where the elements of \mathbf{W} are

$$W_{nm, n' m'} = W_{nn}^D \delta_{m, m'} + W_{mm'}^D \delta_{n, n'} + \gamma W_{nm, n' m'}^R . \tag{35}$$

An estimate of the reaction time scale may be obtained from the eigenvalues of the birth-death processes described by the matrix \mathbf{W}^R as follows:

$$|\lambda_j^R| = \frac{\|\mathbf{W}^R \mathbf{g}_j\|}{\|\mathbf{g}_j\|} \leq \max_{\mathbf{g}} \frac{\|\mathbf{W}^R \mathbf{g}\|}{\|\mathbf{g}\|} = \|\mathbf{W}^R\| , \tag{36}$$

where \mathbf{g}_j is an eigenvector labeled by the index j and the vector norm $\|\cdot\|$ may be chosen in any convenient way. For a vector norm $\|(x_1, \dots, x_N)\| = \sum |x_i|$, the corresponding matrix form is

$$\|\mathbf{W}\| = \max_j \sum_i |W_{ij}| . \tag{37}$$

The chemical relaxation time determined by $|\lambda_1^R|$, the largest chemical relaxation rate, should be slower than that corresponding to the diffusion relaxation eigenvalue λ_1^D ; thus, $\|\mathbf{W}^R\|/|\lambda_1^D| = N\|\mathbf{W}^R\| \ll 1$.

Diffusion tends to homogenize the system; it breaks the correlations between the A and B species induced by reaction and leads to a local binomial distribution of molecules at a site. Provided the chemical reaction is a slow process one might expect the site distribution to be approximately binomial, characterized by the local particle density. In view of this we may construct the analog of a normal solution [13] to the Markov chain (34). We write the full distribution as the sum of a binomial distribution plus a correction term

$$\mathbf{P}(\mathbf{r}, t) = \mathbf{p}^B(\mathbf{c}(\mathbf{r}, t)) + \gamma \Phi(\mathbf{r}, t) \quad , \quad (38)$$

where

$$p_{nm}^B(\mathbf{c}(\mathbf{r}, t)) = p_n^B(a(\mathbf{r}, t)) p_m^B(b(\mathbf{r}, t)) \quad , \quad (39)$$

is a product of binomial distributions for the two species characterized by their local densities. The local densities $\mathbf{c}(\mathbf{r}, t) = (a(\mathbf{r}, t), b(\mathbf{r}, t))$ are as yet unknown quantities. The function Φ and the densities are determined from Eq. (34) and the solvability conditions

$$\sum_{n,m} \Phi_{nm} = 0 \quad , \quad \sum_{n,m} n \Phi_{nm} = 0 \quad , \quad \sum_{n,m} m \Phi_{nm} = 0 \quad . \quad (40)$$

Substituting Eq. (38) into Eq. (34) and using the solvability conditions leads to equations for the local densities to order γ

$$\begin{aligned} a(\mathbf{r}, t+1) - a(\mathbf{r}, t) &= D_A \Delta a(\mathbf{r}, t) + R_A(\mathbf{c}(\mathbf{r}, t)) \quad , \\ b(\mathbf{r}, t+1) - b(\mathbf{r}, t) &= D_A \Delta b(\mathbf{r}, t) + R_B(\mathbf{c}(\mathbf{r}, t)) \quad . \end{aligned} \quad (41)$$

This is just the reaction-diffusion equation where the reaction fluxes are given by

$$\begin{aligned} R_A(\mathbf{c}(\mathbf{r}, t)) &= \sum_{nm, n'm'} n W_{nm, n'm'}^R p_{n'm'}^B \quad , \\ R_B(\mathbf{c}(\mathbf{r}, t)) &= \sum_{nm, n'm'} m W_{nm, n'm'}^R p_{n'm'}^B \quad , \end{aligned} \quad (42)$$

and have the same mass-action forms given earlier. Scaling of space, time, and concentration variables gives the FitzHugh-Nagumo reaction-diffusion equation.

The deviations from the binomial distribution and the relaxation to it can be found by computing Φ which satisfies the equation,

$$\Phi(\mathbf{r}, t+1) - \Phi(\mathbf{r}, t) = \mathbf{W}^D \Phi(\mathbf{r}, t) + \mathbf{S}(\mathbf{r}, t) \quad , \quad (43)$$

where

$$\mathbf{S}(\mathbf{r}, t) = \left(\mathbf{W}^R \mathbf{p}^B - \frac{\partial \mathbf{p}^B}{\partial \mathbf{c}} \cdot \mathbf{R} \right) \quad . \quad (44)$$

Note that

$$\sum_{n,m} n S_{nm} = \sum_{n,m} m S_{nm} = 0 \quad . \quad (45)$$

Thus, $n S_{nm}$ and $m S_{nm}$ are reactive flux deviations whose means are zero. These fluxes act as source terms that drive

the deviations from the local binomial distribution. Considering the local densities as fixed parameters on the fast time scale of relaxation of Φ , the solution of Eq. (43) subject to the initial condition $\Phi(t=0) = \mathbf{S}$ is

$$\Phi(\mathbf{r}, t) = \sum_{j=0}^t (1 + \mathbf{W}^D)^j \mathbf{S} \quad . \quad (46)$$

The characteristic relaxation rate for \mathbf{W}^D in this equation is λ_1^D so that deviations from the local binomial distribution relax rapidly and the reaction-diffusion description will be valid provided $N \|\mathbf{W}^R\| \ll 1$ as discussed above.

V. MICROSCOPIC SIMULATIONS OF CHEMICAL PATTERNS

In Sec. IV we demonstrated that the microscopic dynamics reduces to the reaction-diffusion equation if relaxation to the local binomial distribution is rapid compared to chemical and diffusion time scales and the distribution function is accurately represented by a product of binomial distributions characterized by the local species densities. If these conditions are met fluctuations and correlations will be small and the spatial and temporal scales of the phenomena of interest will be large compared to microscopic scales, such as the lattice spacing or the discrete time step. In this regime we expect the microscopic simulations to reproduce results obtained by the reaction-diffusion equation, and this serves as a test of the microscopic model in this limiting regime. In this section we demonstrate that a number of different types of patterns predicted to exist on the basis of the reaction-diffusion equation are observed in simulations of the microscopic model.

The phenomenology of the FHN reaction-diffusion equation is very rich: it possesses regimes of excitability, oscillations and bistability and their associated wave processes. Rather than reproducing all of this behavior, which we have verified can be examined in the context of the microscopic model, we focus on the bistable regime. Within this bistable regime we further limit our demonstrations to three examples: Ising and Bloch fronts in two spatial dimensions and stable knots and links in three dimensions.

The Ising regime is characterized by the existence of a single front solution connecting the two stable states. In this regime, for small enough diffusion ratio $\delta = D_B/D_A$, one observes domain coarsening like model A of critical phenomena [14] or its vector order parameter analog [15], although there is no free energy functional for small ϵ values. For larger δ , stable stripe structures exist. If δ exceeds a critical value, the planar front may become unstable to transverse perturbations and a labyrinthine pattern will form. Figure 3 shows a lattice-gas simulation for an asymmetric situation where the two bistable states do not have the same stability. The simulation starts from a stripe of the less-stable phase (dark gray, referred to as phase 1) in a sea of the more-stable phase (light gray, referred to as phase 2). The transverse instability amplifies small fluctuations and the planar front kinkles. Small internal fluctuations play a negligible role in the subsequent evolution. The stripe folds and then undergoes a fingering instability clearly seen in the second and third panels. This process continues until the laby-

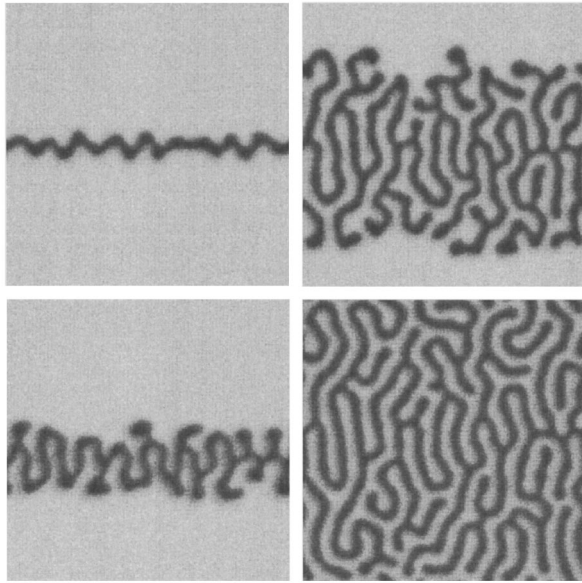


FIG. 3. Evolution of a labyrinthine pattern from a stripe initial condition. The concentration of species A is shown. Dark regions correspond to the less-stable state. Panels (top to bottom and left to right) correspond to times 30ks (1000 automation steps = 1ks = 48.4), 60ks, 250ks. Mean-field parameter values of Eq. (2) are $\epsilon=0.017$, $\alpha=3.05$, $\beta=0.146$, and $\delta=4$. Simulations were carried out on a 1024×1024 lattice.

rinthine pattern fills the entire periodic domain. Note that the dark gray domain of phase 1 is connected but quite complicated. As a result of the diffusive coupling through the B field across the domains, whose boundaries are characterized by sharp variations of the A field, domains do not fuse and the resulting labyrinthine pattern is stable and stationary.

Microscopic structure underlies these apparently smooth chemical patterns. In Fig. 4 we show a labyrinthine pattern that formed from a random distribution with average density corresponding to the unstable state. Since the parameters are such that the two stable states are equivalent, the dark and light domains occupy equal areas. In addition, the pattern is fragmented and the domains of one color are not fully connected since the random initial state evolves to disconnected patches of each phase that deform and lock into the observed state as a result of front repulsion. The right panel shows a

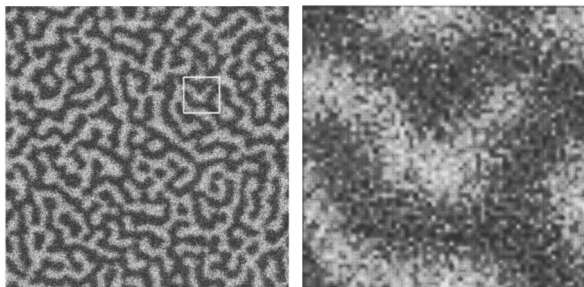


FIG. 4. Fully developed labyrinthine pattern. In the left panel concentration of species B is shown as shades of gray. In the right panel an enlargement of the region marked by the white border is presented to display the local particle distribution. Mean-field parameter values of Eq. (2) are $\epsilon=0.157$, $\alpha=2.92$, $\beta=0.0$, and $\delta=4$. Simulations were carried out on a 512×512 lattice.

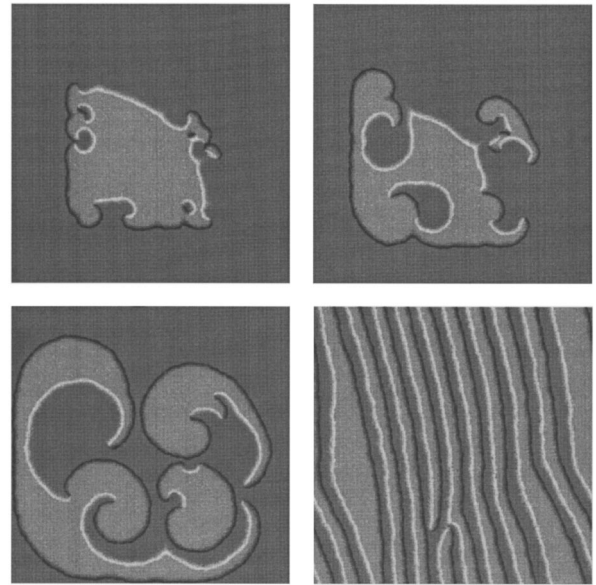


FIG. 5. Evolution of patterns in Bloch regime. Intensity of gray is proportional to $n+2m$. “Dark” fronts are propagating toward low concentration of A and “light” fronts are moving toward low concentration of B . Panels (left to right and top to bottom) correspond to times 10ks (1ks = 95.3), 20ks, 40ks, 1.5Ms. Mean-field parameter values of Eq. (2) are $\epsilon=0.084$, $\alpha=4.88$, $\beta=0.0$, and $\delta=0$. Simulations were carried out on a 1024×1024 lattice.

magnification of one portion of the pattern where small, microscopic fluctuations can be seen.

In the Bloch regime the v field is displaced relative to the u field and counterpropagating fronts exist [16,4]. This implies, even for equistable states of phase 1 and phase 2, that it is possible for phase 1 to consume phase 2 and vice versa, depending on the initial conditions. Consequently, if no front instabilities are possible, one may form arrays of traveling stripes or spiral waves. Figure 5 shows the development of such Bloch fronts from a quadrant of a disk of phase 1 in a sea of phase 2. The two equistable phases are color coded as phase 1 (light gray) and phase 2 (darker gray). The color coding has also been selected to display the two types of front in this regime. One sees that part of the interfacial zones are black, indicating that phase 1 consumes phase 2, while other parts of the interfacial zone are white, indicating that phase 2 consumes phase 1. This is the signature of Bloch fronts [4]. If δ is large enough to exceed the transverse instability threshold, spiral turbulence may develop. We have also observed such spiral turbulence in our simulations.

In three spatial dimension more complicated patterns are possible [17]. One may find parameter regions where tubular segments filled with the less-stable phase embedded in a sea of the more-stable phase are stable. These are the three-dimensional analogs of the stable spot solutions found earlier in two dimensions [3]. It is possible to bend these tubular regions into various shapes such as rings, links, or knots. Two factors are important in determining the stabilities of the resulting objects: the tendency for fronts to “repel” so that domain fusion is prevented, and the tendency of the system to reduce the curvature in the chemical pattern. As a result of competition between these two effects it is possible to topologically stabilize patterns. An example is given in

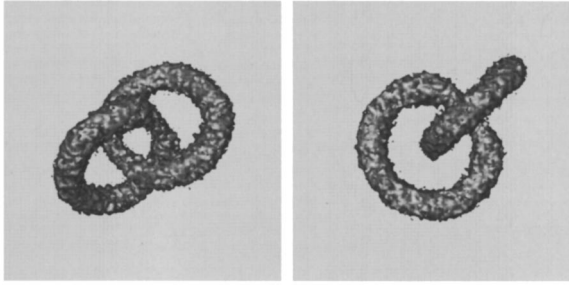


FIG. 6. A stable Hopf link. The concentration of species B is coded by gray shades with black corresponding to high concentration and white to low concentration. The initial condition had the topology of a Hopf link composed of linear tubular segments. Mean-field parameter values of Eq. (2) are $\epsilon=0.0055$, $\alpha=5.21$, $\beta=0.329$, and $\delta=4$. Simulations were carried out on a $256 \times 128 \times 128$ lattice.

Fig. 6 which shows a stable Hopf link. Under the given system conditions a single ring will shrink to a stable ball, but two rings that form a Hopf link are stable since further shrinkage is prevented by domain repulsion.

Another example of topological stabilization is provided by knotted patterns. Figure 7 shows a stable figure-8 knot. Again the tubular domain is filled with the less-stable phase and is embedded in a sea of the more-stable phase. Now the connectivity of the knot in conjunction with domain repulsion prevents shrinkage to ball resulting in a stable knot. A discussion of these three-dimensional patterns is given in Ref. [17].

This brief section has simply served to demonstrate that under appropriate conditions the microscopic FHN model is able to produce even the complex phenomenology of the reaction-diffusion equations. As such, it may serve as a powerful, stable, simulation method to explore the phenomena in regimes that may be difficult for direct simulations of the reaction-diffusion equations; for example, in complicated geometries. However, since the model does incorporate internal molecular fluctuations, we now turn to an exploration of the effects of such fluctuations on the pattern formation processes.

VI. FLUCTUATIONS AND CHEMICAL PATTERNS

In Sec. IV we showed that the macroscopic reaction-diffusion equation will adequately describe the dynamics if

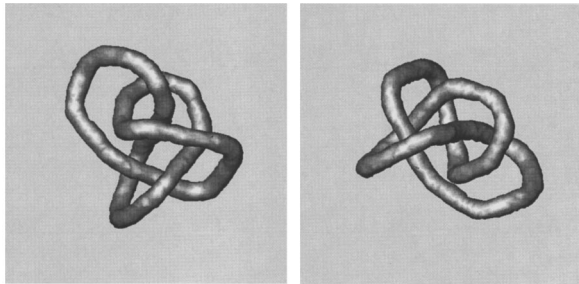


FIG. 7. Two projections of the figure-8 knot. Mean-field parameter values of Eq. (2) are $\epsilon=0.0137$, $\alpha=5.06$, $\beta=0.202$, and $\delta=4$. Simulations were carried out on a $256 \times 256 \times 256$ lattice with slightly different diffusion rules.

diffusion dominates reaction, so that a local equilibrium description is valid. The results in the preceding section demonstrated this numerically. It is interesting to examine the effects of increasing the overall reaction rate, relative to that for diffusion, to study how the macroscopic model breaks down for fast reactions. The overall reaction rate is controlled by the scale factor γ in Eq. (10). The factor γ gauges the ratio of the diffusion to reaction time scales. Making this scaling explicit the reaction diffusion equation reads,

$$\frac{\partial \mathbf{c}(\mathbf{r}, t)}{\partial t} = \gamma \mathbf{R}(\mathbf{c}(\mathbf{r}, t)) + \mathbf{D} \nabla^2 \mathbf{c}(\mathbf{r}, t) . \quad (47)$$

Clearly, within the description provided by this equation, variations in γ can be accounted for by the time and space rescalings, $\bar{t} = t\gamma$ and $\bar{r} = r\sqrt{\gamma}$, respectively. Thus, we may vary γ at fixed system parameters, ϵ , α , β , and δ and probe the breakdown of Eq. (47).

A. Stationary probability distribution

Before examining pattern formation processes, we consider the stationary, single-site, probability distribution P_{nm}^s function as a function of γ . This distribution determines the nature of the single-site reactive correlations between the A and B species and underlies the behavior seen on longer distance scales. Consequently, it is of interest to first examine its structure.

As an example, consider system parameters corresponding to the symmetric bistable regime of the FHN model with zero B diffusion coefficient, $D_B=0$. In the simulations presented below we vary γ and examine how the site probability density changes. The site probability distribution function was numerically computed by determining the occupancies of all sites on the lattice after a transient period where the system was allowed to relax to the statistically stationary regime.

As discussed in Sec. IV, in the limit of large diffusion the stationary probability distribution is binomial, characterized by the average particle density. In the bistable regime, the mean-field model yields two stable steady states. In the fluctuating medium noise-induced transitions between these stable states are possible and the stationary probability density is bimodal with well-separated sharp maxima at the steady states, provided transitions are rare events. In this case the stationary probability density may be approximated by a product of binomial distributions, each characterized by one of the two steady state concentrations. The top left panel of Fig. 8 shows the numerically computed probability density. In this simulation the dynamics in the entire spatial domain remained in the vicinity of a single steady state and no nucleation of the second phase or noise-induced transition processes were observed. As a result the probability density is peaked about one of the steady states and we have verified that it is binomial to a good approximation.

In the other extreme, where diffusion is zero and sites on the lattice do not communicate, the stationary probability is determined by the stationary solution of Eq. (26). This equation is difficult to solve analytically but from its structure one may conclude that the distribution does not factor into a product of functions for the A and B species and it is not

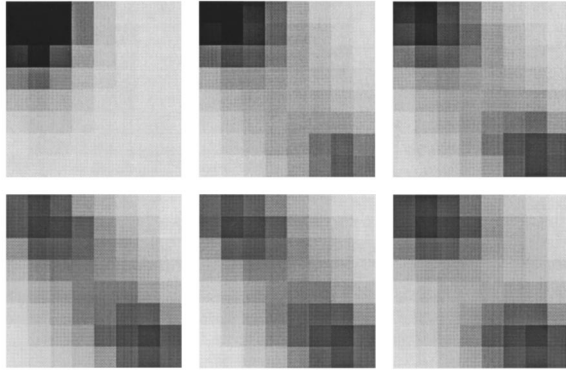


FIG. 8. Stationary probability distributions for different reaction to diffusion ratios are shown. The abscissa and ordinate of each panel are n and m , respectively, which lie in the range $[0,7]$. Panels (left to right and top to bottom) show the change of the stationary probability distributions from a binomial distribution to a correlated distribution determined by the stationary solution of Eq. (26). Reaction rate constants are $k_1=0.98$, $k_2=0.1$, and $k_3=0.2$. Mean-field parameter values of Eq. (2) are $\epsilon=0.13$, $\alpha=3.89$, and $\beta=0.0$. Panels correspond to the γ values $\{0.27, 0.45, 0.47, 0.59, 0.64, 0.97\}$.

binomial. The results of simulations are shown in the lower right panel of Fig. 8 and confirm these conclusions concerning the structure of the distribution. Note that it is bimodal but the density maxima do not correspond to the mean-field steady state values. Thus, new noisy steady states arise from the reactive correlations between the two species.

The remaining intermediate panels of Fig. 8 show the site probability density functions for various values of γ . Now domains of the two phases exist and this is reflected in the bimodal character of the distributions. One observes that as diffusion increases, moving from the bottom right panel to the upper left panel, the bimodal distribution seen for zero diffusion deforms and ultimately leads to the large diffusion case described above.

B. Modification and destruction of patterns

Since, variations in γ can be viewed as time and space rescalings in the reaction-diffusion equation, as γ increases the spatial scales of any chemical patterns will decrease and ultimately approach the mesoscopic scales where fluctuation effects begin to play a role. Also, diffusion will not completely destroy the local reactive correlations. For these large γ values a number of new phenomena are possible, including spontaneous nucleation of domains of one phase in the other and fluctuation-induced alteration or even destruction of chemical patterns.

As an illustration of the effect of increasing γ on chemical pattern formation consider the evolution of a labyrinthine pattern from a stripe initial condition discussed earlier. We consider the same system parameters as Fig. 3 but now γ is larger by a factor of $5/3$. Figure 9 shows the evolution of the labyrinth in this case. The color coding is similar to that in Fig. 3 with dark gray denoting the less-stable state and light gray the more-stable state. One observes several new features in this figure. The fluctuations create domains of supercritical nuclei of the (dark) less-stable phase. Due to the front instability, these deform to form segments of a labyrinthine pattern. Fluctuations may also be strong enough to fragment

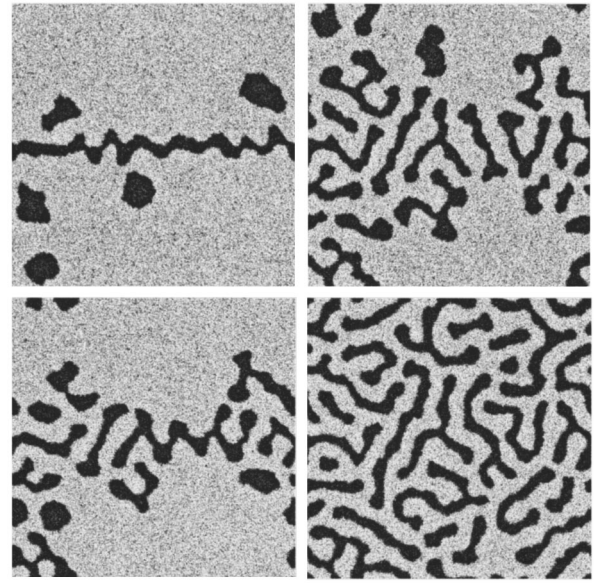


FIG. 9. Effect of small noise on labyrinthine pattern formation. Parameters are identical to those of Fig. 3 but with reaction scaled by $5/3$. Simulations were carried out on a 512×512 lattice.

the initial linelike structure, giving rise to additional segments that tend to form labyrinthine patterns. In the late stages of the evolution, when the labyrinth occupies all space, nucleation is strongly suppressed. However, the labyrinthine pattern is not stationary as in the deterministic system for these parameter values: noise induces transitions among a family of labyrinthinelike states, with segments fusing and breaking as a result of fluctuations.

If γ is sufficiently large, fluctuations may completely destroy the chemical pattern. In Fig. 10 we show passage from a labyrinthine pattern to a disordered state by scaling the reaction rate by factors of 2. When domains become thin front interfaces become diffuse and transitions that change the structure of the pattern become frequent. The characteristic domain width is the same in all panels as a result of space scaling by $\sqrt{2}$. The condition $L_\lambda \gg 1/\sqrt{2d}$ (cf. the end of Sec. IVA) is satisfied even when breakdown of the chemical pattern is observed. Thus, the breakdown is not due to a violation of the condition on the diffusion relaxation time. In the labyrinth regime the reaction-diffusion system possesses multiple steady states comprised of patterns with different topologies. As noise increases transitions between these states become more frequent and the labyrinth pattern is destroyed, although the intrinsic correlation length persists to higher noise levels.

C. Noise-induced phase transitions

We now show the relation between the breakdown of the reaction-diffusion description and noise-induced phase transitions. We consider bistable media with two equistable phases. The simulations suggest the existence of two distinct types of second and first order phase transitions.

For zero B diffusion, $D_B=0$, and large values of ϵ , the density of species B is a fast variable and channels employing B particles may be adiabatically eliminated from the microscopic model. The resulting scheme possesses a free energy functional. In this case the concentration of either

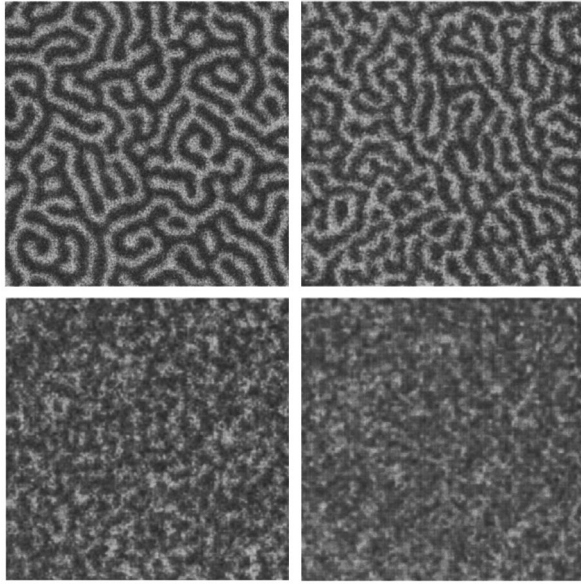


FIG. 10. Transition from a labyrinth to a disordered state. The panels (left to right and top to bottom) show the results of sequential scaling of reaction coefficients by factor of 2. The spatial dimensions by are scaled $\sqrt{2}$ and the results recorded at the same scaled time so that deviations among the panels can be ascribed to breakdown of the reaction-diffusion equation (47). Reaction transition probabilities used in (10) are $k_1=0.98$, $k_2=0.1$, $k_3=0.2$, and $\delta=4.0$. Panels (left to right and top to bottom) correspond to scaling coefficients $\gamma=(0.6, 1.2, 2.4, 4.8)$, respectively.

species serves as an order parameter and in the bistable regime the transition is continuous. The transition occurs as the system becomes inhomogeneous through spontaneous nucleation events.

When the states are not well separated, or diffusion is weak, there is a high probability of the spontaneous nucleation of long-lived domains of the second phase in the sea of dominant phase. Thus, in simulations we observed that, near critical transitions, fluctuations strongly affect local stationary probability distributions. An essential feature of the phase transition process is the reactive correlations between A and B species that build up at a node when diffusion is not infinite. As a result, as demonstrated in Fig. 8, the site distribution is not binomial. These local correlations propagate to neighboring lattice nodes and are eventually destroyed by diffusion. Consequently, the character of the local fluctuations is affected by the nature of the species site correlations, and any description of the destruction of patterns and phase transitions must account for the buildup of these local correlations.

Consider the evolution of the probability distribution governed by the Markov chain (34) with \bar{a} approximated by the average particle density in the entire system, which is equivalent to an average over the probability distribution. In this case, the evolution of the probability density is given by

$$\mathbf{P}(t+1) - \mathbf{P}(t) = \tilde{\mathbf{W}}(\mathbf{c}(t))\mathbf{P}(t), \quad \mathbf{c}(t) = \sum_{n,m} (n,m)P_{nm}(t) \quad (48)$$

where \mathbf{c} is a vector of average species concentrations. We use the symbol $\tilde{\mathbf{W}}$ for \mathbf{W} in Eq. (35) with \bar{a} and \bar{b} replaced

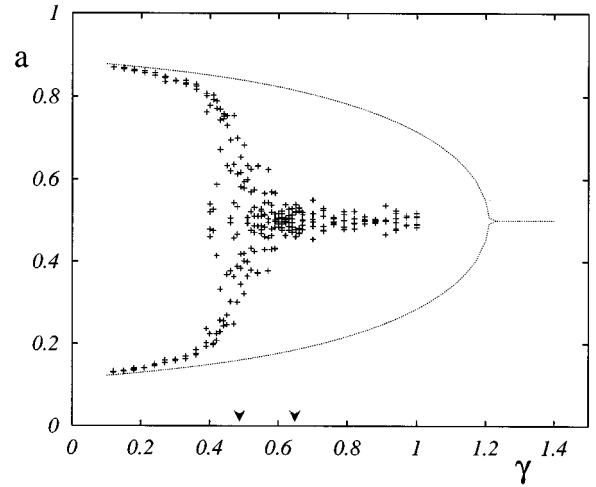


FIG. 11. Lattice-gas simulations (+) and mean-field theory results (dotted line) for a system showing a second order phase transition as γ varies. The ordinate is the global density of species A . System parameters are the same as in Fig. 8. The arrows indicate γ values where the system spatial distribution is shown in Fig. 12. Simulations were carried out on a 256×256 lattice.

by the the average concentrations of A and B . While this simple mean-field description of the diffusion process neglects details of spatial correlations among sites, it correctly describes the creation of correlations at a site by reactive events. The diffusion in model is exact for an infinite-dimensional system.

The mean-field results are given by the stationary solutions of Eq. (48). In Fig. 11 we present the average particle density as a function of γ . The plot shows a pitchfork bifurcation characteristic of second order phase transitions. The simulation points were obtained by monitoring the global density of species A as a function of time within the statistically stationary regime. Six points widely separated in time are plotted for each value of γ . Below the transition, for large values of γ , these points are randomly distributed about the unstable steady state $(a,b)=(1/2,1/2)$. Above the transition, the system switches between the two stable phases. Thus, in this region the stationary probability density is sharply peaked about the deterministic steady state values, with very small density between these density maxima.

Deviations of mean-field results from the simulations may be attributed to the existence of long range correlations near the critical transition. The ratio of mean-field and computed γ_{crit} values is close to that of the Ising model. This supports the assumption that the shift in the transition point is due to the neglect of spatial information in the mean-field diffusion model. In Fig. 12 domains corresponding to different reaction-diffusion ratios near the transition are shown. The domain sizes decrease as γ increases and this leads to the above-mentioned breakdown of the mean-field description.

The microscopic model does not possess a conserved order parameter and we expect the system to be close to model A of critical phenomena under the conditions described above. In Fig. 13 we present results for the spatial correlation functions obtained during evolution from an unstable state. Dynamical scaling results obtained from the assumption of

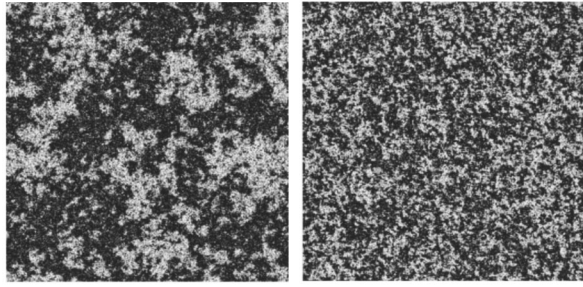


FIG. 12. Snapshots of domains near the second order phase transition. Values of the scaling coefficient γ are marked in Fig. 11 by arrows.

curvature-driven coarsening yields a scaling exponent of 0.5 [18]. In this case the scaling form is

$$C(r,t) = \frac{r}{q(t)} C\left(\frac{r}{q(t)}\right), \quad \text{with } q(t) \sim \sqrt{t} \quad (49)$$

where $q(t)$ is a characteristic domain length. The collapse of the correlation function confirms the assumed form of the character of the coarsening.

We note that in general the FitzHugh-Nagumo model does not have a free energy functional and thus the correspondence with model A is not complete. In Fig. 14 we present results of simulations in a different regime where the mass-action fixed points are less well separated. The results suggest the existence of a first order phase transition. In this case the plot of the average particle density does not follow a continuous path as a function of γ but displays a sharp jump.

The origin of such behavior may be understood within the mean-field approximation. The time evolution of the average particle density is shown in Fig. 15 for various diffusion-reaction ratios indicated by arrows in Fig. 14. For the largest γ value, $\gamma=3.3$, the system spirals to the stable focus at $(a,b)=(1/2,1/2)$ (finely dotted line in Fig. 15). We observe that above the first critical point, when steady state bifurcates

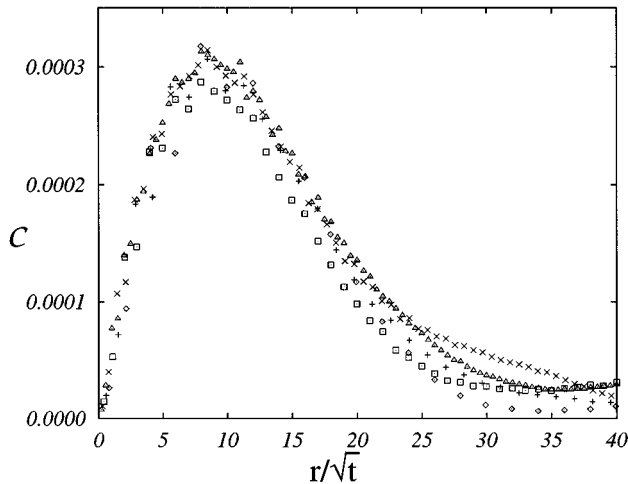


FIG. 13. Collapse of spatial correlation functions obtained in the course of annealing from a deep quench. System parameters are the same as in Fig. 8 and correspond to a scaling coefficient $\gamma=0.2$.

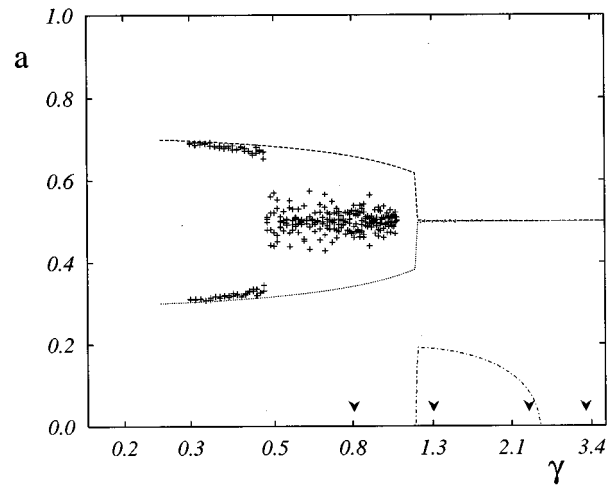


FIG. 14. Noise-induced first order phase transition. Results of lattice-gas simulations (+) and mean-field theory (dashed line) are displayed. The lowest (dotted-dashed line) curve shows the amplitude of the mean-field density oscillations. Trajectories of mean-field densities for values marked by arrows are shown in Fig. 15. Reaction transition probabilities used in Eq. (10) are $k_1=0.82$, $k_2=0.167$, and $k_3=0.133$. Mean-field parameter values of Eq. (2) are $\epsilon=0.38$, $\alpha=1.45$, and $\beta=0.0$. Simulations were carried out on a $64 \times 64 \times 64$ lattice.

into a stationary cycle, there are no self-consistent stable solutions of the system (48). In this case the average particle density of the system oscillates around the average value $(1/2,1/2)$ and the stationary symmetric probability distribution transforms into a rotating probability distribution after this Hopf bifurcation. For the two chosen γ values in this region, one observes limit cycle behavior. There is a small-amplitude limit cycle at $\gamma=2.3$ (dashed line), which grows to a large limit cycle at $\gamma=1.3$ (solid line). Subsequently, at

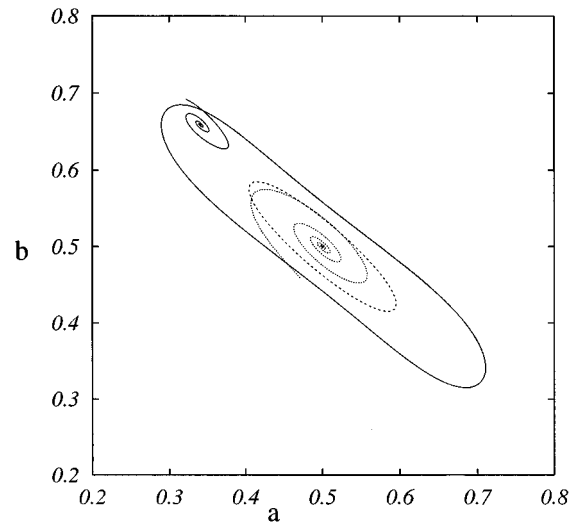


FIG. 15. Trajectories of the mean-field average densities computed from Eq. (48) corresponding to the γ values $\{0.8, 1.3, 2.3, 3.3\}$. System parameters are identical with those of Fig. 14. See text for details.

$\gamma=1.2$, the cycle collapses to the stable points which, in turn, evolve to the mean-field values. Evolution to the stable focus at $\gamma=0.8$ is shown as a solid line in Fig. 15.

The absence of a self-consistent stationary solution of the mean-field approximation requires discussion. In a large spatially distributed system the picture of an oscillating probability density seems to be unrealistic. The cycle has finite period and synchronization of an infinite system during one period is improbable. Instead, there are random oscillating patches of varying phases distributed over system. In this case the average particle density is given by the “unstable” solution of system (48). In the spatially distributed system undergoing bifurcation from a bistable state to a steady cycle, the noise takes anomalously large values due to the existence of domains of different phases [19]. This accounts for the wide distribution of the stroboscopic trajectory points shown in Fig. 14.

The critical phenomena discussed above do not give a complete picture of the possible phase transitions in the model but do provide insight into the possible types of system behavior. A full description must properly account for nonlocal correlations as well as the local reactive correlations.

VII. SUMMARY

The two-species reaction scheme that leads to the FitzHugh-Nagumo mass-action rate law implies a local reactive collision dynamics, which was used to investigate this system from a microscopic point of view. The fact that the reaction scheme depends on both the particle occupancies and their vacancies means that the scheme may be implemented without approximation as lattice-gas automaton with exclusion. As a result, large scale computations on parallel computers are especially efficient [20] and have made fea-

sible three-dimensional simulations of complex structures such as links and knots [17].

The Markov chain model that underlies the lattice-gas implementation was described and the conditions needed to yield the diffusion, mass-action, and reaction-diffusion equations were discussed. These considerations also provide a means to investigate the breakdown of the macroscopic models.

In appropriate limits the model was shown to reproduce the chemical patterns seen in reaction-diffusion models with FitzHugh-Nagumo kinetics. However, utilizing the fact that the model is microscopic, the effects of fluctuations on pattern formation and the breakdown of mean-field and reaction-diffusion descriptions were studied. In particular, as the reaction rate increases relative to diffusion, the local equilibrium description was shown to break down. Chemical patterns are destroyed and noise-induced phase transition phenomena were observed. The character and order of the phase transformations depends on the parameter regime.

The present paper by no means completes the study of internal fluctuations on pattern formation processes in this dynamical system. Since the macroscopic model does not, in general, possess a free energy functional, an especially rich variety of phenomena are possible. We have focussed solely on the bistable regime and considered only a few examples of pattern formation processes. Other regimes, such as the oscillatory and excitable regimes, may now be studied from a microscopic point of view using the model and techniques developed here. Through the use of such models one may gain insight into the statistical mechanics of spatially distributed, far-from-equilibrium, reacting systems.

ACKNOWLEDGMENTS

This work was supported in part by a grant from the Natural Sciences and Engineering Research Council of Canada.

-
- [1] R. FitzHugh, *Biophys. J.* **1**, 445 (1961); J. Nagumo, S. Arimoto, and Y. Yoshikawa, *Proc. IRE* **50**, 2061 (1962).
- [2] See, for instance, M. Courtemanche, W. Skaggs, and A. T. Winfree, *Physics D* **41**, 173 (1990); A. T. Winfree, *Chaos* **1**, 3031 (1991); A. T. Winfree, *SIAM Review* **32**, 1 (1990) and references therein.
- [3] T. Ohta, A. Ito, and A. Tetsuka, *Phys. Rev. A* **42**, 3225 (1990); T. Ohta, R. Mimura, and M. Kobayashi, *Physica D* **34**, 115 (1989).
- [4] A. Hagberg and E. Meron, *Phys. Rev. Lett.* **72**, 2494 (1994); C. Elphik, A. Hagberg, and E. Meron, *Phys. Rev. E* **51**, 3052 (1995).
- [5] D. M. Petrich and R. E. Goldstein, *Phys. Rev. Lett.* **72**, 1120 (1994); R. E. Goldstein, D. J. Muraki, and D. M. Petrich, *Phys. Rev. E* **53**, 3933 (1996).
- [6] K. J. Lee, W. D. McCormack, Q. Ouyang, and H. L. Swinney, *Science* **261**, 192 (1993); K. J. Lee and H. L. Swinney, *Phys. Rev. E* **51**, 1899 (1995); K. J. Lee, W. D. McCormack, J. Pearson, and H. L. Swinney, *Nature* **214**, 215 (1994).
- [7] A cellular automaton model to simulate reaction-diffusion equations was constructed by J. Weimar and J.P. Boon, *Phys. Rev. E* **49**, 1749 (1994), and applied to the FHN model in J. Weimar, D.Sc. thesis, Brussels (1995). The cellular automaton is not deduced from a microscopic dynamics.
- [8] See, for example, B. Alberts, D. Bray, J. Lewis, M. Raff, K. Roberts, and J. D. Watson, *The Molecular Biology of the Cell* (Garland, New York, 1983).
- [9] M. Eiswirth and G. Ertl, in *Chemical Waves and Patterns*, edited by R. Kapral and K. Showalter (Kluwer, Dordrecht, 1995), and references therein.
- [10] J. P. Boon, D. Dab, R. Kapral, and A. Lawniczak, *Phys. Rep.* **273**, 55 (1996).
- [11] U. Frisch, D. d’Humières, B. Hasslacher, P. Lallemand, Y. Pomeau, and J.P. Rivet, *Complex Syst.* **1**, 649 (1987).
- [12] C. W. Gardiner, *Handbook of Stochastic Processes* (Springer-Verlag, New York, 1985).
- [13] S. Chapman and T. G. Cowling, *Mathematical Theory of Non-Uniform Gases* (Cambridge University Press, Cambridge, England, 1952).
- [14] P. C. Hohenberg and B. I. Halperin, *Rev. Mod. Phys.* **49**, 435 (1977).
- [15] A. J. Bray and S. Puri, *Phys. Rev. Lett.* **67**, 2670 (1991); H. Toyoki, *Phys. Rev. B* **45**, 1965 (1992).
- [16] P. Coulet, J. Lega, B. Houchmanzadeh, and J. Lajzerowich,

- Phys. Rev. Lett. **65**, 1352 (1990).
- [17] A. Malevanets and R. Kapral, Phys. Rev. Lett. **77**, 767 (1996).
- [18] J. Gunton and M. Droz, *Introduction to the Theory of Metastable and Unstable States*, Vol. 183 of *Lecture Notes in Physics* (Springer-Verlag, New York, 1983).
- [19] J. Keizer, *Statistical Thermodynamics of Nonequilibrium Processes* (Springer-Verlag, New York, 1987).
- [20] N. Margolus, in *Pattern Formation and Lattice-Gas Automata*, edited by R. Kapral and A. Lawniczak (Fields Institute Communications, AMS, Providence, 1996), p.165.